Gauge-independent decoherence models for solids in external fields

Michael S. Wismer[*] and Vladislav S. Yakovlev
Max-Planck-Institut für Quantenoptik, Hans-Kopfermann-Straße 1, Garching 85748, Germany
and Ludwig-Maximillian Universität, Geschwister-Scholl-Platz 1, München 80539, Germany

(Received 3 December 2017; revised manuscript received 27 March 2018; published 17 April 2018)

We demonstrate gauge-invariant modeling of an open system of electrons in a periodic potential interacting with an optical field. For this purpose, we adapt the covariant derivative to the case of mixed states and put forward a decoherence model that has simple analytical forms in the length and velocity gauges. We demonstrate our methods by calculating harmonic spectra in the strong-field regime and numerically verifying the equivalence of the deterministic master equation to the stochastic Monte Carlo wave-function method.

DOI: 10.1103/PhysRevB.97.144302

I. INTRODUCTION

Real-time numerical modeling of light-solid interaction is one of the key theoretical tools for studying novel nonlinear phenomena, such as high-harmonic generation [1,2]. One of the challenges here is modeling decoherence caused by the interaction of electrons with their environment. Especially for highly nonlinear processes, an *ab initio* description of this interaction is currently out of reach, and a phenomenological description of decoherence is therefore common. Care has to be taken when it is used in conjunction with *ab initio* electronic-structure data, and the nature of the problems that need to be addressed depends on the chosen electromagnetic gauge. The two most popular choices are the length and velocity gauges.

In the length gauge, the interaction Hamiltonian contains the coordinate operator. In the basis of stationary Bloch states, this operator becomes what is known as the crystal-coordinate operator, which involves differentiation with respect to crystal momentum [3]. Evaluating this derivative is problematic when Bloch states are obtained numerically because eigenstates of a Hamiltonian are defined only up to random phase factors. For pure states, this problem was successfully solved by the so-called covariant derivative [4–6] (related methods include link operators [7] and a generalized derivative [8–10]). This method, however, cannot be directly applied to mixed states—the covariant derivative needs to be adapted for simulations with decoherence.

The velocity gauge obviates the necessity to differentiate with respect to crystal momentum. However, it is important to consider gauge invariance while implementing a particular decoherence model in the velocity gauge [11,12]. On the one hand, gauge invariance is frequently used as an essential test in numerical simulations. On the other hand, phenomenological relaxation terms that are known to work well in the length gauge may lead to unphysical results when they are used verbatim in the velocity gauge [13]. A brute-force solution to this problem is to combine velocity-gauge propagation with length-gauge decoherence, performing gauge transformations at each step of numerical propagation [11]. Because these transformations are time consuming, and also because velocity-gauge simulations usually require a large basis set for convergence [10,14,15], it is desirable to have more efficient gauge-independent decoherence models.

In this paper, we examine gauge-invariant modeling of optical excitations in the presence of decoherence. For length-gauge calculations, we generalize the derivative operator for mixed states. We then consider a subclass of Lindblad-type dephasing models that are well suited for gauge-invariant numerical modeling. Addressing the issue of high computational costs of density-matrix calculations, we demonstrate a successful velocity-gauge implementation of the Monte Carlo wave-function (MCWF) method [16]. As a practical example, we apply our methods to the problem of high-harmonic generation in a one-dimensional periodic potential.

II. MASTER EQUATION

We start by considering the Hamiltonian of a particle of mass m and charge q in a local potential subject to a classical, homogeneous electric field:

$$\hat{H}(t) = \frac{[\hat{\mathbf{p}} - q\mathbf{A}(t)]^2}{2m} + V(\hat{\mathbf{r}}) + q\phi(\hat{\mathbf{r}},t). \tag{1}$$

The gauge-dependent potentials are related to the electric field via

$$\mathbf{E}(t) = -\left(\nabla\phi(\mathbf{r},t) + \frac{\partial\mathbf{A}(t)}{\partial t}\right), \tag{2}$$

where the potentials in the length and velocity gauges can be expressed as four-vectors:

$$(\phi_{\mathrm{LG}},\mathbf{A}_{\mathrm{LG}}) = (-\mathbf{E}(t)\cdot\hat{\mathbf{r}},\mathbf{0}), \tag{3}$$

$$(\phi_{\mathrm{VG}},\mathbf{A}_{\mathrm{VG}}) = \left(0, -\int_{-\infty}^{t}\mathbf{E}(t')\,dt'\right). \tag{4}$$

The unitary operator $\hat{U} = \exp[iq\mathbf{A}(t)\cdot\hat{\mathbf{r}}/\hbar]$ transforms the Hamiltonian from the length gauge to the velocity gauge, i.e., $\hat{U}(\hat{H}[\phi_{\mathrm{LG}},\mathbf{A}_{\mathrm{LG}}] - i\hbar\partial_t)\hat{U}^\dagger = \hat{H}[\phi_{\mathrm{VG}},\mathbf{A}_{\mathrm{VG}}]$.

[*]michael.wismer@mpq.mpg.de

We now denote the field-free Hamiltonian as $\hat{H}_0$ and introduce the crystal momentum $\mathbf{k}$:

$$\hat{H}_{0,\mathbf{k}} = e^{-i\mathbf{k}\cdot\hat{\mathbf{r}}}\hat{H}_0 e^{i\mathbf{k}\cdot\hat{\mathbf{r}}}. \tag{5}$$

The eigenstates $\hat{H}_{0,\mathbf{k}}|u^0_{i\mathbf{k}}\rangle = E_{i\mathbf{k}}|u^0_{i\mathbf{k}}\rangle$ constitute a convenient basis of spatially periodic functions in which we can expand time-dependent solutions:

$$|u_{i\mathbf{k}}(t)\rangle = \sum_j^{N_b} |u^0_{j\mathbf{k}}\rangle c_{ji\mathbf{k}}(t). \tag{6}$$

We describe interactions with the environment using the Lindblad superoperator,

$$\hat{\mathcal{L}}(\hat{\rho}) = \hat{L}\hat{\rho}\hat{L}^\dagger - \tfrac{1}{2}(\hat{L}^\dagger\hat{L}\hat{\rho} + \hat{\rho}\hat{L}^\dagger\hat{L}), \tag{7}$$

and solve the master equation:

$$i\hbar\partial_t\hat{\rho} = [\hat{H}(t),\hat{\rho}] + i\hat{\mathcal{L}}(\hat{\rho}). \tag{8}$$

The Lindblad formalism has the advantage of preserving the trace and positiveness of the density matrix. We are interested in modeling decoherence using a Lindblad operator that can be expressed analytically irrespective of the gauge. To this end, we can use operators of the form

$$\hat{L}_{\mathrm{LG}} = f(\hat{\mathbf{p}}, \hat{H}_0), \tag{9}$$

where f is an arbitrary operator function. For a homogeneous electric field, we can use $\hat{\mathbf{p}} = -i\hbar\nabla$ to express the Lindblad operator in the velocity gauge as

$$\begin{aligned}\hat{L}_{\mathrm{VG}} &= f(\hat{U}\hat{\mathbf{p}}\hat{U}^\dagger, \hat{U}\hat{H}_0\hat{U}^\dagger)\\ &= f\left(\hat{\mathbf{p}} - q\mathbf{A}(t), \hat{H}_0 - \frac{q}{m}\mathbf{A}\cdot\hat{\mathbf{p}} + \frac{q^2}{2m}A^2(t)\right).\end{aligned} \tag{10}$$

Having a Lindblad operator that is exact in both gauges simplifies the analysis of gauge invariance. We will use the following simple form of the decoherence operator:

$$\hat{L}_{\mathrm{LG}} = \sqrt{\gamma}\hat{H}_0. \tag{11}$$

Since this expression does not depend on $\hat{\mathbf{p}}$, it commutes with $\hat{H}_0$; consequently, this type of decoherence does not have a direct effect on the energy of the system. By combining Eqs. (7) and (11), we get

$$\mathcal{L}_{\mathrm{LG}}(\hat{\rho}_{\mathrm{k,LG}})_{ij} = -(\gamma/2)(E_{i\mathbf{k}} - E_{j\mathbf{k}})^2(\rho_{\mathbf{k},\mathrm{LG}})_{ij}. \tag{12}$$

This expression describes the decay of off-diagonal elements of the density matrix at rates that depend on the difference between the energies. Although we do not attempt to describe the physical origin of decoherence rates with this particular scaling, energy-dependent decoherence is, in general, to be expected [17]. Energy-dependent dephasing rates were employed to obtain better agreement with experimental results [18,19]. Note that coherence between degenerate states does not decay in our case.

In the velocity gauge, the decoherence operator (11) reads

$$\hat{L}_{\mathrm{VG}} = \sqrt{\gamma}\left(\hat{H}_{0,\mathbf{k}} - \frac{q}{m}\mathbf{A}\cdot\hat{\mathbf{p}}_{\mathbf{k}} + \frac{q^2}{2m}A^2(t)\right). \tag{13}$$

Correspondingly, the master equation (8) becomes

$$\begin{aligned}i\hbar\partial_t\rho_{\mathbf{k},\mathrm{VG}} &= [H_{0,\mathbf{k}} + q\mathbf{A}(t)\cdot\mathbf{p}_{\mathbf{k}}, \rho_{\mathbf{k},\mathrm{VG}}]\\ &\quad + i(\gamma/2)\Bigg[H_{0,\mathbf{k}} - \frac{q}{m}\mathbf{A}(t)\cdot\mathbf{p}_{\mathbf{k}},\\ &\quad \times\left[\rho_{\mathbf{k},\mathrm{VG}}, H_{0,\mathbf{k}} - \frac{q}{m}\mathbf{A}(t)\cdot\mathbf{p}_{\mathbf{k}}\right]\Bigg].\end{aligned} \tag{14}$$

Here and in the following, we drop the hat above operators whenever the meaning is clear. We note that terms proportional to $A^2(t)$ disappear since scalars commute with operators. An attractive feature of the velocity gauge is that density matrices at different $\mathbf{k}$ points are independent of one another.

The master equation in the length gauge reads

$$\begin{aligned}i\hbar\partial_t\rho_{\mathbf{k},\mathrm{LG}} &= [H_{0,\mathbf{k}} + iq\mathbf{E}(t)\cdot\partial_{\mathbf{k}}, \rho_{\mathbf{k},\mathrm{LG}}]\\ &\quad + i(\gamma/2)[H_{0,\mathbf{k}}, [\rho_{\mathbf{k},\mathrm{LG}}, H_{0,\mathbf{k}}]],\end{aligned} \tag{15}$$

where $\hat{\mathbf{r}} \to i\partial_{\mathbf{k}}$ upon transformation to reciprocal space [3]. Care has to be taken when calculating the derivative because Bloch functions are not necessarily smooth functions of $\mathbf{k}$. For a set of pure states uniformly occupying the valence bands, one can define the covariant derivative [4,5] by considering parallel transport of a single nondegenerate Bloch function or a subspace of degenerate Bloch functions from one $\mathbf{k}$ point to a neighboring one. The covariant derivative, herewith denoted as $\tilde{\partial}_{\mathbf{k}}$, can also be used for explicitly evaluating dipole transition elements between nondegenerate Bloch functions:

$$(\mathbf{d}_{\mathbf{k}})_{ij,\alpha} = \langle u^0_{i\mathbf{k}}|\tilde{\partial}_{\mathbf{k}}|u^0_{j\mathbf{k}}\rangle_\alpha = \frac{S^0_{\mathbf{k},\mathbf{k}+\Delta\mathbf{k}_\alpha ij}}{S^0_{\mathbf{k},\mathbf{k}+\Delta\mathbf{k}_\alpha jj}} - \frac{S^0_{\mathbf{k},\mathbf{k}-\Delta\mathbf{k}_\alpha ij}}{S^0_{\mathbf{k},\mathbf{k}-\Delta\mathbf{k}_\alpha jj}}, \tag{16}$$

where $(S^0_{\mathbf{k},\mathbf{k}+\Delta\mathbf{k}_\alpha})_{ij} = \langle u^0_{i\mathbf{k}}|u^0_{j\mathbf{k}+\Delta\mathbf{k}_\alpha}\rangle$. Later on, we will also use the notation $(S_{\mathbf{k},\mathbf{k}+\Delta\mathbf{k}_\alpha})_{ij} = \langle u_{i\mathbf{k}}|u_{j\mathbf{k}+\Delta\mathbf{k}_\alpha}\rangle$. We note that these matrix elements are consistent with dipole transition elements evaluated as $(\mathbf{d}_{\mathbf{k}})_{ij,\alpha} = (iq\hbar/m_e)(\mathbf{p}_{\mathbf{k}})_{ij,\alpha}/(E_{i\mathbf{k}} - E_{j\mathbf{k}})$.

Generalizations of parallel transport for mixed systems were discussed by Uhlmann [20] and Sjöquist [21]. For a system of mixed states of Bloch functions, as considered here, a decomposition into orthogonal states at every $\mathbf{k}$ point can be conducted: $\rho_{\mathbf{k}} = \sum_{ij} C_{ij\mathbf{k}}|u^0_{i\mathbf{k}}\rangle\langle u^0_{j\mathbf{k}}| = \sum_n p_{n\mathbf{k}}|\tilde{u}_{n\mathbf{k}}\rangle\langle\tilde{u}_{n\mathbf{k}}|$. Since $p_{n\mathbf{k}}$ is a continuous variable, it is in principle possible to track changes in every of state as it varies over $\mathbf{k}$ and calculate the parallel transport between a pair of states at neighboring $\mathbf{k}$ points, i.e., between $|\tilde{u}_{n\mathbf{k}}\rangle$ and $|\tilde{u}_{n\mathbf{k}+\Delta\mathbf{k}_\alpha}\rangle$. This approach, however, is straightforward only as long as the decomposition is unique, which is not the case if degenerate values of $p_{n\mathbf{k}}$ occur. For practical calculations, we instead propose to approximate the derivative as

$$\begin{aligned}[\partial_{\mathbf{k}}, \rho_{\mathbf{k},\mathrm{LG}}] &= (2\pi N_k)^{-1}\sum_\alpha N_\alpha\mathbf{R}_\alpha\\ &\quad\times(\tilde{\rho}_{\mathbf{k}+\Delta\mathbf{k}_\alpha,\mathrm{LG}} - \tilde{\rho}_{\mathbf{k}-\Delta\mathbf{k}_\alpha,\mathrm{LG}})\,\tilde{\rho}_{\mathbf{k},\mathrm{LG}} - \mathrm{H.c.},\end{aligned} \tag{17}$$

where $\mathbf{R}_\alpha$ denotes lattice vectors, N_α is the number of $\mathbf{k}$ points along the corresponding reciprocal vector, $N_k = \prod_\alpha N_\alpha$ is the total number of $\mathbf{k}$ points in the Brillouin zone, and where we have introduced $\tilde{\rho}_{\mathbf{k}} = \sum_n \sqrt{p_{n\mathbf{k}}}|\tilde{u}_{n\mathbf{k}}\rangle\langle\tilde{u}_{n\mathbf{k}}|$ which ensures linearity of the commutator in the limit $\Delta\mathbf{k} \to 0$. In our

numerical calculations, we evaluated $\tilde{\rho}_{\mathbf{k}}$ using singular-value decomposition. The changes in the coefficients of the density matrices $C_{ij\mathbf{k},\mathrm{LG}} = \langle u^0_{i\mathbf{k}}|\rho_{\mathbf{k},\mathrm{LG}}|u^0_{j\mathbf{k}}\rangle$ in the basis of field-free eigenstates are then calculated as

$$\begin{aligned}&\langle u^0_{i\mathbf{k}}|\tilde{\rho}_{\mathbf{k}+\Delta\mathbf{k}_\alpha,\mathrm{LG}}\tilde{\rho}_{\mathbf{k},\mathrm{LG}}|u^0_{j\mathbf{k}}\rangle \\ &\quad = \left(S^0_{\mathbf{k},\mathbf{k}+\Delta\mathbf{k}_\alpha}\,\tilde{C}_{\mathbf{k}+\Delta\mathbf{k}_\alpha,\mathrm{LG}}\,S^{0\dagger}_{\mathbf{k},\mathbf{k}+\Delta\mathbf{k}_\alpha}\,\tilde{C}_{\mathbf{k},\mathrm{LG}}\right)_{ij},\end{aligned} \tag{18}$$

where $\tilde{C}_{ij\mathbf{k},\mathrm{LG}} = \langle u^0_{i\mathbf{k}}|\tilde{\rho}_{\mathbf{k},\mathrm{LG}}|u^0_{j\mathbf{k}}\rangle$. The dipole transition elements that can be derived from Eq. (17) coincide with those derived from Eq. (16) in the case of a complete basis set where $(S^0_{\mathbf{k},\mathbf{k}+\Delta\mathbf{k}_\alpha})^\dagger = (S^0_{\mathbf{k},\mathbf{k}+\Delta\mathbf{k}_\alpha})^{-1}$. In the limit $\Delta\mathbf{k}_\alpha \to 0$, the terms $\langle u^0_{i\mathbf{k}+\Delta\mathbf{k}_\alpha}|u^0_{j\mathbf{k}}\rangle$ approach Kronecker deltas up to irrelevant phase factors if none of the Bloch states are degenerate.

Having laid out the formalism for determining the dynamics using deterministic equations in both gauges, we note that decoherence can also be modeled by means of the Monte Carlo wave-function method (MCWF) [16]. This method replaces the problem of propagating all N_b^2 elements of a density matrix by propagating N_v valence-band functions, each containing N_b elements. This scaling makes it computationally efficient for systems where the number of conduction bands is significantly larger than the number of valence bands. As velocity-gauge simulations typically require a large number of bands for convergence, the MCWF method is particularly attractive for these simulations. When applying this method, the Bloch functions are propagated from $|u_{i\mathbf{k}}(t)\rangle$ to $|u_{i\mathbf{k}}(t+\Delta t)\rangle$ using the non-Hermitian Hamiltonian:

$$\tilde{H}_{\mathbf{k}} = H_{\mathbf{k}}(t) - \frac{i\hbar}{2}L^\dagger_{\mathbf{k}}(t)L_{\mathbf{k}}(t). \tag{19}$$

The solution is then accepted with probability $\langle u_{i\mathbf{k}}(t+\Delta t)|u_{i\mathbf{k}}(t+\Delta t)\rangle < 1$ and normalized; otherwise, a quantum jump occurs: the propagated function is taken to be $|u_{i\mathbf{k}}(t+\Delta t)\rangle = L_{\mathbf{k}}|u_{i\mathbf{k}}(t)\rangle$ and normalized. As quantum jumps occur independently at different $\mathbf{k}$ points, they cause discontinuities in the excitation densities with respect to $\mathbf{k}$. The velocity gauge is therefore preferable for the MCWF method as Bloch functions at different $\mathbf{k}$ points are propagated independently.

Evaluation of the current

The electric current induced by an external electric field is the key macroscopic observable in the linear and nonlinear optics. The current can be evaluated from the expectation value of the velocity operator:

$$\mathbf{J}_{\mathbf{v}}(t) = \frac{q}{V}\sum_{\mathbf{k}}\mathrm{Tr}[\mathbf{v}_{\mathbf{k}}\rho_{\mathbf{k}}], \tag{20}$$

where $\mathbf{v}_{\mathbf{k}} = [\mathbf{p}_{\mathbf{k}} - q\mathbf{A}(t)]/m$, and V is the unit-cell volume. Alternatively, we can construct the current as the temporal derivative of the polarization obtained from the geometric phase. For each Bloch function, or set of degenerate Bloch functions, the modern theory of polarization [22] provides the following expression:

$$\mathbf{P}(t) = \frac{q}{2\pi V N_k}\sum_{\alpha}\sum_{\mathbf{k}}N_\alpha\mathbf{R}_\alpha\mathrm{Im}\{\ln\det S_{\mathbf{k},\mathbf{k}+\Delta\mathbf{k}_\alpha}\}. \tag{21}$$

For partially occupied bands, it is necessary to generalize Eq. (21) by introducing weights at each $\mathbf{k}$ point:

$$\begin{aligned}\mathbf{P}(t) = \frac{q}{2\pi V N_k}\sum_{\mathbf{k}}\sum_{n}N_\alpha\mathbf{R}_\alpha\sqrt{p_{n\mathbf{k}}p_{n\mathbf{k}+\Delta\mathbf{k}_\alpha}} \\ \times\ \mathrm{Im}\{\ln\det S_{\mathbf{k},\mathbf{k}+\Delta\mathbf{k}_\alpha}\}.\end{aligned} \tag{22}$$

While the polarization is ambiguously defined, the current can be uniquely calculated by taking the temporal derivative of Eq. (21):

$$\mathbf{J}_{\mathrm{GP}}(t) = \frac{q}{2\pi V N_k}\sum_{\mathbf{k}}\sum_{\alpha}N_\alpha\mathbf{R}_\alpha\mathrm{Tr}\left[S^{-1}_{\mathbf{k},\mathbf{k}+\Delta\mathbf{k}_\alpha}\frac{\partial}{\partial t}S_{\mathbf{k},\mathbf{k}+\Delta\mathbf{k}_\alpha}\right]. \tag{23}$$

Equations (20) and (23) are equivalent in the continuum limit ($\Delta\mathbf{k}_\alpha \to 0$), which can easily be shown for pure states. The evaluation of Eq. (23) requires calculating $S^{-1}_{\mathbf{k},\mathbf{k}+\Delta\mathbf{k}_\alpha}$, which is readily done for pure systems. For mixed systems, $S_{\mathbf{k},\mathbf{k}+\Delta\mathbf{k}_\alpha}$ can be singular due to unoccupied states. We therefore evaluate $S^{-1}_{\mathbf{k},\mathbf{k}+\Delta\mathbf{k}_\alpha}$ in Eq. (23) as a normalized pseudoinverse by first performing the singular value decomposition $S = U\Sigma V^\dagger$ and then normalizing the singular values with respect to the $\mathbf{k}$-dependent densities:

$$(Y_{\mathbf{k},\mathbf{k}+\Delta\mathbf{k}_\alpha})_{ii} = \begin{cases} 1/\sqrt{(\Sigma_{\mathbf{k},\mathbf{k}+\Delta\mathbf{k}_\alpha})_{ii}}, & \text{if } (\Sigma_{\mathbf{k},\mathbf{k}+\Delta\mathbf{k}_\alpha})_{ii} \neq 0 \\ 0, & \text{otherwise.}\end{cases} \tag{24}$$

The normalized pseudoinverse is then constructed as

$$\tilde{S}^{-1}_{\mathbf{k},\mathbf{k}+\Delta\mathbf{k}_\alpha} = V_{\mathbf{k},\mathbf{k}+\Delta\mathbf{k}_\alpha}Y_{\mathbf{k},\mathbf{k}+\Delta\mathbf{k}_\alpha}U^\dagger_{\mathbf{k},\mathbf{k}+\Delta\mathbf{k}_\alpha}. \tag{25}$$

III. NUMERICAL RESULTS

Having defined all the necessary equations of motion and the procedures for evaluating observables, we now provide a numerical demonstration of our methods [23]. In the following, we use Hartree atomic units unless stated otherwise. We consider a one-dimensional potential defined as

$$V(x) = -\sum_{n=-\infty}^{\infty}V_0\mathrm{sech}\left(\frac{x - na_{\mathrm{lat}}}{a_0}\right). \tag{26}$$

We calculated Bloch functions by numerical diagonalization of the Hamiltonian in the basis of plane waves. For electrons, we have $m = -q = 1$. Setting the lattice parameters to $V_0 = 1.0$, $a_{\mathrm{lat}} = 5.0$, and $a_0 = 0.2$ leads to a band gap between the two lowest bands of 7.3 eV. The lowest band is taken to be a fully occupied valence band, and the rest are regarded as empty conduction bands. For $\gamma = 0.1$, we get a decoherence time of 6.7 fs at the position of the fundamental band gap. To ensure convergence, we use up to eight bands and up to 800 k points.

The electric field is taken to be a single-cycle Gaussian pulse defined such that the definite integral of the electric field over all times vanishes:

$$E(t) = \frac{E_{\max}}{\omega_0}\frac{d}{dt}\left(e^{-2\ln 2(t^2/t^2_{\mathrm{FWHM}})}\sin(\omega_0 t)\right). \tag{27}$$

Throughout this paper, the electric-field parameters are taken to be $\hbar\omega_0 = 1.6$ eV and $t_{\mathrm{FWHM}} = 2$ fs, so that $\omega_0 t_{\mathrm{FWHM}} \sim \pi$. Field strengths up to $E_{\max} = 1.5$ V/Å are used, which

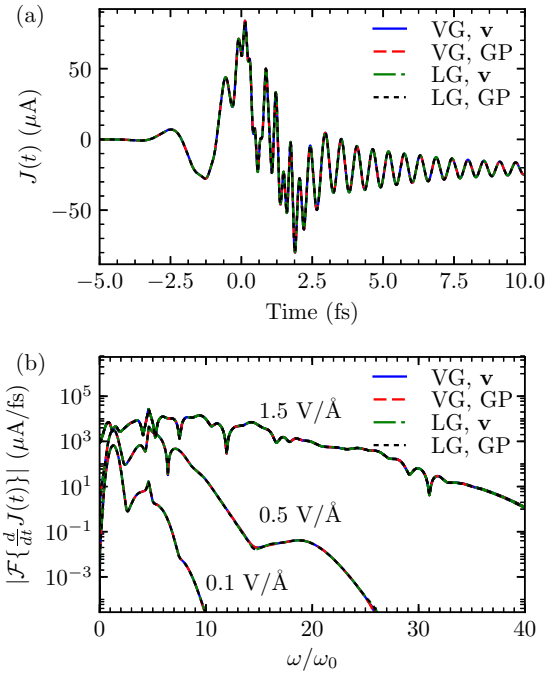

FIG. 1. (a) Time-resolved induced current for the ground state subjected to a pulse with a peak electric-field strength of 1.5 V/Å. (b) Power spectrum of the acceleration for pulses of varying peak field strength. In both plots, the results for the length gauge (LG) (blue, red) and velocity gauge (VG) (green, black) and for currents obtained via the velocity operator (**v**) (blue, green) and the geometric phase (GP) (red, black) are practically identical.

is sufficiently strong to accelerate electrons across half the Brillouin zone, i.e., $eE_{\max}a_{\text{lat}}/\hbar\omega_0 \sim \pi$.

Figure 1 shows the optical nonlinear response evaluated using four different methods: we propagated the density matrix using the length and velocity gauges and, in both cases, we evaluated the electric current density once with Eq. (20) and once with Eq. (23). All four models shown in Fig. 1 give visually indistinguishable responses for all of the field strengths used.

Figure 1(a) shows that the current oscillates rapidly during the laser pulse and decays to a constant value after the external field vanishes. The oscillations after the laser pulse are due to the coherent superpositions of conduction- and valence-band states. The visibly more rapid oscillations during the laser pulse are due to the interaction of excitations with the external field. This high-frequency content of the polarization response is clearly visible in Fig. 1(b), where we show optical spectra as the Fourier transform of the time derivative of the current. The single-cycle laser pulse that we chose for this numerical example does not generate distinct harmonic peaks. Nevertheless, the spectra in Fig. 1(b) show several features characteristic to high harmonics in solids. For example, several plateaus emerge due to the presence of multiple conduction bands [24]; the plateau between $15\omega_0$ and $25\omega_0$ in the calculation with $E_{\max} = 0.5$ V/Å disappears if we use only one conduction band in our length-gauge simulations (not shown).

Figure 2 shows the distributions of electrons in the lowest three conduction bands at the end of the laser pulse. This figure further confirms the gauge independence of our calculations.

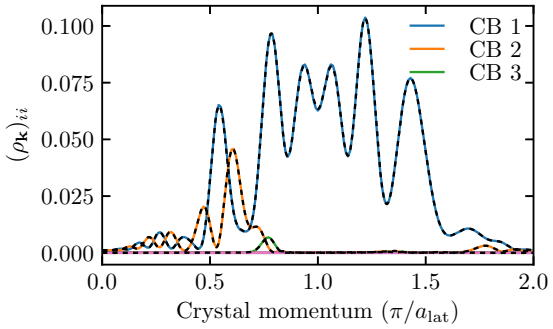

FIG. 2. Distributions of electrons in the conduction bands (CBs) after excitation by a pulse with $E_{\max} = 1.5$ V/Å according to a velocity gauge calculation (colored, solid lines) and length gauge calculation (black, dashed lines).

A comparison of MCWF results to those obtained using the deterministic methods is shown in Fig. 3. For the chosen field strength of 1.5 V/Å, the spectrum in Fig. 3(b) converges fast for photon energies up to $\approx 20\omega_0$. Because of the high field strength, the peak at the fundamental frequency splits into two separate peaks [25]. As quantum jumps lead to discontinuities

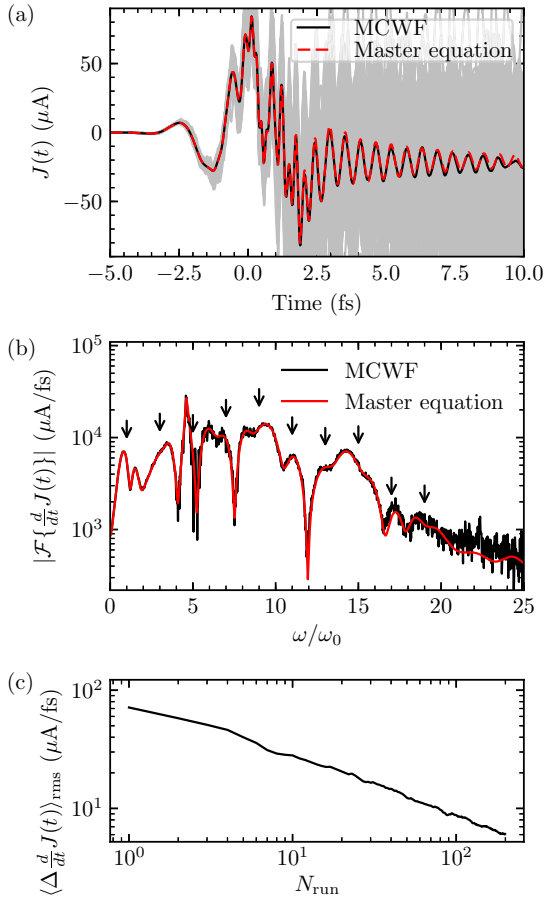

FIG. 3. (a) Current obtained from MCWF method and the exact solution obtained by solving the master equation for a field strength of 1.5 V/Å. Currents obtained from individual runs are shown in gray. (b) Spectrum of the acceleration with arrows indicating the expected location of the odd harmonics. (c) Root-mean-square deviation from the exact result as a function of the number of individual runs.

in the observables or their derivatives, their frequency spectra contain noisy components. Consequently, it is necessary to take an average over many runs, and we average the optical response over 200 runs to obtain a reasonably converged spectrum. As expected, the results converge as $\sqrt{N_{\rm run}}$, and this behavior is observed in Fig. 3(c). The method is therefore less suited for analyzing low-magnitude high-frequency components. As only eight bands were necessary for convergence in our one-dimensional example, the MCWF method did not outperform the master equation approach in terms of computational time.

IV. DISCUSSION

The excellent agreement between the results obtained in the length and velocity gauges confirms the validity of our proposed method for differentiating mixed states in reciprocal space [see Eq. (17)]. The method can readily be applied to two- and three-dimensional solids and is therefore applicable to *ab initio* data obtained from, e.g., density-functional-theory calculations. Furthermore, our numerical results confirm that constructing decoherence (and relaxation) operators as functions of $\mathbf{p}$ and H is beneficial as it alleviates issues with gauge transformations. This, however, requires a sufficiently complete basis, where the sum rules are satisfied and Eq. (10) holds.

Our approach can also be generalized to approximate experimentally observed excitation-dependent decoherence rates [26]. Whenever an external electric field is present, $(\rho_{\rm VG})_{ii} \neq (\rho_{\rm LG})_{ii}$ and it is therefore more convenient to express the excitation in terms of absorbed energy. For a ground state with energy $E_{\rm gs}$ and band gap $E_{\rm g}$, the density can be approximated as $n_{\rm exc} \approx [\sum_{\mathbf{k}} \langle H_{\mathbf{k}}(t)\rangle - E_{\rm gs}]/E_{\rm g}$. In this approach, there is no reference to gauge-dependent quantities, and no transformation between gauges is necessary. In order to make decoherence rates scale with the cubic root of the conduction-band density, one can use the following Lindblad operator: $L_{\mathbf{k}} = \tilde{\gamma}[\sum_{\mathbf{k}} \langle H_{\mathbf{k}}(t)\rangle - E_{\rm gs}]^{1/3} H_{\mathbf{k}}(t)$.

Further work is, however, necessary to define a universal scheme that treats nonlocal potentials [27,28], inhomogeneous fields, as well as corrections to the single-particle equation of motion arising from scattering and many-body effects on equal footing in all gauges. Our demonstration of the equivalence of the two gauges in systems subject to decoherence can be used for testing the validity of approximations that may break gauge invariance. Finally, we note that, in our implementation, velocity-gauge calculations are faster than the length-gauge ones, while evaluating the current from the expectation value of the velocity operator is faster than evaluating it from the geometric phase. For parallelization over $\mathbf{k}$ points, it is preferable to perform simulations in the velocity gauge and evaluate the current density using the velocity operator.

We have also shown that the Monte Carlo wave-function method is very well suited for determining optical properties of condensed matter in the velocity gauge, except for resolving very high-frequency components.

ACKNOWLEDGMENTS

M.S.W. was supported by the International Max Planck Research School of Advanced Photon Science. V.S.Y. was supported by the DFG Cluster of Excellence: Munich-Centre for Advanced Photonics.

APPENDIX A: PHYSICAL MEANING OF THE INVESTIGATED DECOHERENCE OPERATOR

With Eq. (9), we introduced a class of decoherence (relaxation) operators that possess convenient numerical properties. We did not derive this form of a Lindblad operator from first principles. Nevertheless, it should be possible to approximate a particular microscopic model of dephasing with a model that complies with Eq. (9). For simplicity, we considered the case $L \propto H_0$. In this section, we examine the physical meaning of this choice.

Let us consider a system of electrons interacting with a bath of bosons described by an annihilation operator b_n and a creation operator $b_n^\dagger$. In the absence of an external electric field, the Hamiltonian of the combined system is then

$$\mathcal{H} = H_0 + \sum_n \mathcal{E}_n b_n^\dagger b_n + \sum_n H_0(\gamma_n b_n^\dagger + \gamma_n^* b_n),$$

where H_0 describes Bloch electrons, $\sum_n \mathcal{E}_n b_n^\dagger b_n$ governs the dynamics of the bath, and $H_I = \sum_n H_0(\gamma_n b_n^\dagger + \gamma_n^* b_n)$ describes the interaction of electrons with the bosonic bath. We will assume that the bath is sufficiently large to neglect the influence of electrons on it. Transforming the Hamiltonian into the interaction picture with respect to the bath yields

$$\begin{aligned}\mathcal{H} &= H_0 + \sum_n H_0(\gamma_n b_n^\dagger e^{i\mathcal{E}_n t} + \gamma_n^* b_n e^{-i\mathcal{E}_n t}),\\ &\approx H_0\left[1 + 2\sum_n |\gamma_n|\sqrt{N_n}\cos(\mathcal{E}_n t + \arg\gamma_n)\right]\\ &= H_0[1+\eta(t)],\end{aligned} \tag{A1}$$

where $\eta(t)$ is a fluctuating function that depends on the coupling strengths γ_n; we have denoted bath eigenvalues with $\mathcal{E}_n$ and occupation numbers with $N_n \gg 1$. Within the approximation encoded in Eq. (A1), the effect of the bath on the system is to multiply the energies with $\lambda(t) = 1 + \eta(t)$. Such a modulation can result from the uniform deformation of a lattice potential:

$$\begin{aligned}H_{\lambda(t)} &= \frac{-\hbar^2}{2m}\nabla_{\mathbf{r}}^2 + \lambda(t) V(\sqrt{\lambda(t)}\mathbf{r})\\ &= \lambda(t)\left[\frac{-\hbar^2}{2m}\nabla_{\mathbf{s}}^2 + V(\mathbf{s})\right],\end{aligned} \tag{A2}$$

where $\mathbf{s} = \sqrt{\lambda(t)}\mathbf{r}$. If Bloch functions adiabatically follow changes of the lattice potential, their energies will be modulated with $\lambda(t)$. This may serve as a very rough model of a breather mode of lattice vibrations. It should, however, be kept in mind that a Kohn-Sham potential V contains, in addition to the bare lattice potential, the Hartree and exchange-correlation potentials from the other electrons.

The function $\eta(t)$ represents the time-dependent, stochastic deformation of the potential, where the randomness arises from the phase of the complex-valued coupling factors γ_n. In the limiting case of a stochastic function with a white noise spectrum, averaging over all possible realizations of $\eta(t)$ yields $\langle \eta(t)\rangle_\eta = 0$ and $\langle \eta(t)\eta(t')\rangle_\eta \propto \delta(t-t')$. For each realization of

$\eta(t)$, the wave functions can formally be propagated in time as

$$|\psi_n(t+\Delta t)\rangle = \mathcal{U}(t+\Delta t,t)|\psi_n(t)\rangle \tag{A3}$$

$$\approx \left(1 - \frac{i}{\hbar}H_0\Delta t - \frac{i}{\hbar}H_0\int_t^{t+\Delta t} dt'\eta(t') - \frac{1}{\hbar^2}H_0^2\int_t^{t+\Delta t} dt'\int_t^{t'} dt''\eta(t')\eta(t'')\right)|\psi_n(t)\rangle, \tag{A4}$$

where we have kept only terms where Δt appears in the first order. The evolution of the density matrix can then be determined from

$$\begin{aligned}
\rho(t+\Delta t) &= \left\langle \sum_n |\psi_n(t+\Delta t)\rangle\langle\psi_n(t+\Delta t)| \right\rangle_\eta \\
&= \langle \mathcal{U}(t+\Delta t,t)\rho(t)\mathcal{U}^\dagger(t+\Delta t,t)\rangle_\eta \\
&\approx \left\langle \left(1 - \frac{i}{\hbar}H_0\Delta t - \frac{i}{\hbar}H_0\int_t^{t+\Delta t} dt'\eta(t') - \frac{1}{\hbar^2}H_0^2\int_t^{t+\Delta t} dt'\int_t^{t'} dt''\eta(t')\eta(t'')\right)\right. \\
&\quad \times \rho(t)\left(1 + \frac{i}{\hbar}H_0\Delta t + \frac{i}{\hbar}H_0\int_t^{t+\Delta t} dt'\eta(t') - \frac{1}{\hbar^2}H_0^2\int_t^{t+\Delta t} dt'\int_t^{t'} dt''\eta(t')\eta(t'')\right)\Bigg\rangle_\eta \\
&\approx \rho(t) - \frac{i}{\hbar}[H_0,\rho(t)]\Delta t \\
&\quad + \frac{\gamma}{2}\left(H_0\rho(t)H_0 - \frac{1}{2}H_0^2\rho(t) - \frac{1}{2}\rho(t)H_0^2\right)\Delta t.
\end{aligned} \tag{A5}$$

At the last step, we dropped terms quadratic with respect to Δt and assumed

$$\left\langle \int_t^{t+\Delta t} dt'\int_t^{t'} dt''\eta(t')\eta(t'')\right\rangle_\eta = \frac{\hbar^2\gamma}{4}\Delta t. \tag{A6}$$

Comparing Eq. (A5) to master equations (14) and (15), we see that the stochastic multiplicative perturbation of the Hamiltonian, encoded in Eq. (A1), leads to the decoherence operator that we introduced with Eq. (11).

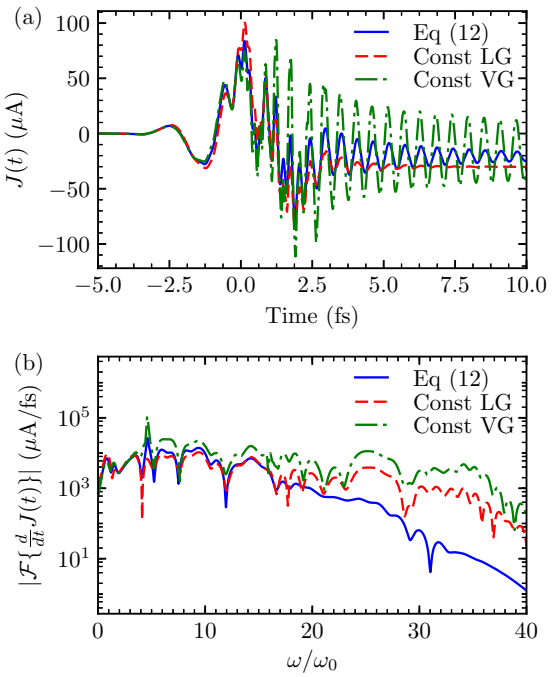

FIG. 4. Optical current Master equation evaluated with the dephasing rates given in Eq. (12) (blue), and evaluated using constant dephasing rates in length gauge (red) and velocity gauge (green). (a) Time domain and (b) spectral domain.

APPENDIX B: UNIFORM DECOHERENCE RATES

In this appendix, we illustrate the violation of gauge invariance when formally the same expression for decoherence is used in the length and velocity gauges. For this example, we chose the case where all states dephase at the same rate in the length gauge: $\mathcal{L}_{\rm LG}(\rho)_{ij} = \gamma_0\rho_{ij}(1-\delta_{ij})$ where δ_{ij} is the Kronecker symbol. In the velocity gauge, we use the same dephasing terms, $L_{\rm VG}(\rho) = L_{\rm LG}(\rho)$. The dephasing rate is taken to be $\gamma_0 = (0.47\ {\rm fs})^{-1}$, which corresponds to the energy-dependent dephasing rate evaluated at the average energy difference between the valence band and lowest conduction band. As the dephasing terms are not gauge invariant, the two master equations do not correspond to the same physical system, so the dielectric response is expected to be visibly different. The outcomes of solving the master equation with these new terms are shown in Fig. 4. The time-dependent electric currents are visibly different. In the spectral domain, the two new energy-independent dephasing models produce spectral intensities that significantly exceed that presented in the main text, especially at the high frequencies ($\omega > 25\omega_0$).

[1] D. Golde, T. Meier, and S. W. Koch, Phys. Rev. B **77**, 075330 (2008).
[2] S. Ghimire, A. D. DiChiara, E. Sistrunk, P. Agostini, L. F. DiMauro, and D. A. Reis, Nat. Phys. **7**, 138 (2010).
[3] E. Blount, Solid State Phys. **13**, 305 (1962).
[4] I. Souza, J. Íniguez, and D. Vanderbilt, Phys. Rev. B **69**, 085106 (2004).
[5] C. Attaccalite and M. Grüning, Phys. Rev. B **88**, 235113 (2013).
[6] M. Grüning, D. Sangalli, and C. Attaccalite, Phys. Rev. B **94**, 035149 (2016).

[7] K. S. Virk and J. E. Sipe, Phys. Rev. B **76**, 035213 (2007).
[8] C. Aversa and J. E. Sipe, Phys. Rev. B **52**, 14636 (1995).
[9] T. G. Pedersen, Phys. Rev. B **92**, 235432 (2015).
[10] A. Taghizadeh, F. Hipolito, and T. G. Pedersen, Phys. Rev. B **96**, 195413 (2017).
[11] M. D. Tokman, Phys. Rev. A **79**, 053415 (2009).
[12] D. Sangalli, J. A. Berger, C. Attaccalite, M. Grüning, and P. Romaniello, Phys. Rev. B **95**, 155203 (2017).
[13] W. E. Lamb, Jr., R. R. Schlicher, and M. O. Scully, Phys. Rev. A **36**, 2763 (1987).
[14] J. E. Sipe and Ed Ghahramani, Phys. Rev. B **48**, 11705 (1993).
[15] V. S. Yakovlev and M. S. Wismer, Comp. Phys. Comm. **217**, 82 (2017).
[16] K. Mølmer, Y. Castin, and J. Dalibard, J. Opt. Soc. Am. B **10**, 524 (1993).
[17] M. V. Fischetti and S. E. Laux, Phys. Rev. B **38**, 9721 (1988).
[18] Q. T. Vu, H. Haug, O. D. Mücke, T. Tritschler, M. Wegener, G. Khitrova, and H. M. Gibbs, Phys. Rev. Lett. **92**, 217403 (2004).
[19] F. Langer, M. Hohenleutner, C. P. Schmid, C. Pöllmann, P. Nagler, T. Korn, C. Schüller, M. Sherwin, U. Huttner, J. Steiner *et al.*, Nature (London) **533**, 225 (2016).
[20] A. Uhlmann, Lett. Math. Phys. **21**, 229 (1991).
[21] E. Sjöqvist, A. K. Pati, A. Ekert, J. S. Anandan, M. Ericsson, D. K. L. Oi, and V. Vedral, Phys. Rev. Lett. **85**, 2845 (2000).
[22] R. D. King-Smith and D. Vanderbilt, Phys. Rev. B **47**, 1651 (1993).
[23] We performed our calculations with the `ulmic`-package which is available through GitHub: https://github.com/Wismer255/ulmic.
[24] M. Wu, D. A. Browne, K. J. Schafer, and M. B. Gaarde, Phys. Rev. A **94**, 063403 (2016).
[25] O. D. Mücke, T. Tritschler, M. Wegener, U. Morgner, and F. X. Kärtner, Phys. Rev. Lett. **87**, 057401 (2001).
[26] P. C. Becker, H. L. Fragnito, C. B. BritoCruz, R. R. Fork, J. E. Cunningham, J. E. Henry, and C. V. Shank, Phys. Rev. Lett. **61**, 1647 (1988).
[27] A. F. Starace, Phys. Rev. A **3**, 1242 (1971).
[28] S. Ismail-Beigi, E. K. Chang, and S. G. Louie, Phys. Rev. Lett. **87**, 087402 (2001).